Control of an Underwater Vehicle in Irregular Waves

Thomas Battista and Craig Woolsey
Department of Aerospace & Ocean Engineering
Virginia Tech
Blacksburg, VA 24061
{tomb1, cwoolsey}@vt.edu

Abstract— **In an effort to account for wave forcing in underwater vehicle dynamics, a model derived from Lagrangian mechanics is implemented. The model is first specialized to the case of an underwater vehicle operating in plane progressive waves. A comparison is made between the model in plane progressive waves and an exact solution derived from potential flow theory, revealing that the model accurately captures Froude-Krylov excitation forces. Plane progressive waves are then used to approximate the Pierson-Moskowitz wave energy spectrum as a means to simulate a natural seaway. A proportional derivative (PD) controller is devised to simultaneously maintain a desired depth and heading angle for an underactuated, underwater vehicle to demonstrate the capability of the proposed model.**

I. Introduction

As the state of the art of underwater vehicles trends towards autonomy, the need for more sophisticated models is growing. In the presence of various forms of disturbance, *e.g.* ocean currents and wave excitation forces, an underwater vehicle must be able to execute its prescribed task within reasonable tolerance. Of particular interest is the ongoing challenge of adequately capturing wave forcing in a nonlinear, parametric vessel model that is well suited to control design.

Baily et. al. [1] devised a unified maneuvering and seakeeping model aimed at predicting ship motions in a natural seaway. This work motivated more modern efforts, such as [2] and [3] where the authors present a nonlinear state-space model which incorporates memory effects as an additional state to model radiation forces. Perez then implemented the model for roll control via rudder actuation [3], demonstrating that the model was amenable to control design.

Leonard [4] used geometric mechanics to derive Kirchoff's equations for an underwater vehicle operating in an unbounded, ideal fluid and showed that the dynamics exhibit a Hamiltonian structure. Leonard then applied energy based control techniques in [5] to stabilize steady motions of an underwater vehicle. Woolsey & Techy expand upon this work and use potential shaping to achieve cross track control for an underwater vehicle in [6]. Valentinis et. al. take a similar approach in [7] where they employ a closed loop control law to organize the dynamics into a port-Hamiltonian system and use energy shaping to derive conditions for stable maneuvers.

A nonlinear maneuvering model is presented in [8] parameterized by hydrodynamic derivatives obtained from experimental and computational results. Racine & Paterson [9] employ a sensitivity analysis to identify relevant hydrodynamic derivatives in a maneuvering model and implement an unsteady Reynolds-averaged Navier Stokes (URANS) flow solver to numerically approximate them. It is important to note, however, that these efforts do not account for wave excitation forces.

Thomasson [10] and Thomasson & Woolsey [11] use a Lagrangian approach outlined by Lamb [12] to derive a vehicle model. In this case, the total energy of the fluid-vehicle system is approximated and the resulting equations of motion inherently incorporate forcing terms resulting from arbitrary background fluid motions. The authors in [11] compare this model to analytical potential flow solutions derived for a variety of cases, for instance, a cylinder in proximity of an unsteady source.

This paper specializes the model derived in [11] for the case of an underwater vehicle operating in a natural seaway. While this model does not capture all of the effects that would come with a unified maneuvering and seakeeping model, preliminary results suggest that this simple model does capture some of the essential forcing absent in a standard maneuvering model.

The remainder of the paper is organized as follows. Section II discusses the background theory behind the equations of motion. Section III outlines the formulation of the natural seaway; plane progressive waves are superimposed to model a wave energy density spectrum. The vehicle parameters employed in this paper are given in Section IV and a control problem to demonstrate the proposed model is outlined. Simulations and results for a vehicle operating in plane progressive waves and a natural seaway are also presented and compared in Section IV. Concluding remarks and ongoing work are given in Section V.

II. Equations of Motion

A. Kinematics

Prior to expressing the kinematic equations, several terms are introduced. First, define a set of Earth-fixed axes (i_1, i_2, i_3) where i_3 is aligned with the direction of gravity and i_1 and i_2 exist in the plane defined by i_3. Next, define the body axes (b_1, b_2, b_3) fixed to the vehicle's center of buoyancy in the fore-starboard-down configuration. Let $\boldsymbol{X}$ be the position vector from the origin of the inertial frame to the origin of the body frame and let $\boldsymbol{R}$ define the rotation matrix relating the orientation of the body frame to the inertial

978-0-933957-43-5 ©2015 MTS

frame. Define the translational and rotational velocities $\boldsymbol{v} = (u, v, w)$ and $\boldsymbol{\omega} = (p, q, r)$, respectively, whose components are aligned with (b_1, b_2, b_3). Finally, define the symbol $\hat{\cdot}$ to represent a map from a 3-dimensional vector to a 3-by-3 skew-symmetric matrix satisfying the relationship $\hat{\boldsymbol{\alpha}}\boldsymbol{\beta} = \boldsymbol{\alpha} \times \boldsymbol{\beta}$ for arbitrary vectors $\boldsymbol{\alpha}$ and $\boldsymbol{\beta}$. The kinematic relations are given by

$$\dot{\boldsymbol{X}} = \boldsymbol{R}\boldsymbol{v} \tag{1}$$

$$\dot{\boldsymbol{R}} = \boldsymbol{R}\hat{\boldsymbol{\omega}} \tag{2}$$

B. Dynamics

We briefly divert our attention to introduce the nomenclature in [11] before presenting the equations of motion. Define $\boldsymbol{v}_{\mathrm{f}}(\boldsymbol{X}, \boldsymbol{R}, t)$ to be the background flow field (*i.e.*, excluding the flow induced by the vehicle motion) expressed in the body frame. The flow field can be both unsteady and non-uniform. Let $\boldsymbol{v}_{\mathrm{r}} = \boldsymbol{v} - \boldsymbol{v}_{\mathrm{f}}$ represent the relative velocity vector between the body and the surrounding flow field. The six components of translational and rotational velocities are organized into a single state vector $\boldsymbol{\nu} = (\boldsymbol{v}^T \ \boldsymbol{\omega}^T)^T$. Then the relative velocity state vector is

$$\boldsymbol{\nu}_{\mathrm{r}} = \begin{pmatrix} \boldsymbol{v} - \boldsymbol{v}_{\mathrm{f}} \\ \boldsymbol{\omega} \end{pmatrix}$$

Let $\boldsymbol{M}_{\mathrm{b}}$ denote the 6-by-6 generalized vehicle mass matrix and let $\boldsymbol{M}_f$ denote the added mass and inertia terms. Let $\bar{\boldsymbol{M}} = \mathrm{Diag}(m, m, m, 0, 0, 0)$ where m is the vehicle mass. Define the flow gradient matrix

$$\boldsymbol{\Phi}^T = \left(\frac{\partial \boldsymbol{v}_{\mathrm{f}}}{\partial \boldsymbol{X}} \right) \boldsymbol{R}$$

Finally, let the additional generalized forces and torques to be included in the terms $\boldsymbol{f}$ and $\boldsymbol{\tau}$. We now present equations (13) from [11], the resulting equations of motion from the Lagrangian derivation:

$$\begin{aligned}(\boldsymbol{M}_{\mathrm{f}} + \boldsymbol{M}_{\mathrm{b}})\dot{\boldsymbol{\nu}}_{\mathrm{r}} = &- \begin{pmatrix} \hat{\boldsymbol{\omega}} + \boldsymbol{\Phi} & 0 \\ \hat{\boldsymbol{v}}_{\mathrm{r}} & \hat{\boldsymbol{\omega}} \end{pmatrix} (\boldsymbol{M}_{\mathrm{f}} + \bar{\boldsymbol{M}})\boldsymbol{\nu}_{\mathrm{r}} \\ &+ (\bar{\boldsymbol{M}} - \boldsymbol{M}_{\mathrm{b}}) \begin{pmatrix} \hat{\boldsymbol{v}}_{\mathrm{f}}\boldsymbol{\omega} + \frac{\partial}{\partial t}\boldsymbol{v}_{\mathrm{f}} + \boldsymbol{\Phi}^T\boldsymbol{v} \\ 0 \end{pmatrix} \\ &- \begin{pmatrix} \hat{\boldsymbol{\omega}} & 0 \\ \hat{\boldsymbol{v}} & \hat{\boldsymbol{\omega}} \end{pmatrix} (\boldsymbol{M}_{\mathrm{b}} - \bar{\boldsymbol{M}})(\boldsymbol{\nu}) + \begin{pmatrix} \boldsymbol{f} \\ \boldsymbol{\tau} \end{pmatrix} \end{aligned} \tag{3}$$

Note that in the absence of a background flow field, $\boldsymbol{v}_{\mathrm{f}} = 0$ and $\boldsymbol{\nu}_{\mathrm{r}} = \boldsymbol{\nu}$. In this case, equations (3) reduce to Kirchoff's equations for underwater vehicle motion in an unbounded, ideal fluid.

These equations (3) are a nonlinear system of ordinary differential equations (ODEs) describing the motion of an underwater vehicle subject to an arbitrary flow field. We also draw attention to the fact that these equations can be implemented with relative ease; the only vehicle parameters required are the mass and inertial parameters associated with the vehicle's mass distribution and the added mass and inertia parameters associated with the vehicle hull geometry. The added mass and inertia can be computed using a strip theory code, for instance as outlined in [13].

The remaining terms (excluding those contained with the external forcing terms $\boldsymbol{f}$ and $\boldsymbol{\tau}$) required to initialize the model all derive from the background flow field. There are some restrictions on the background flow field, however, as a result of the approximation of the total system energy used in the Lagrangian derivation. Large scale variations in the flow gradient over the length of the body will result in model error. Examples of this error are given in [11].

III. Wave Formulation

The natural seaway simulated in this paper derives from a potential flow formulation. In potential flow theory, the flow is assumed to be incompressible, inviscid, and irrotational. Under these assumptions, the idealized plane progressive waves can be constructed.

A. Plane Progressive Waves

Plane progressive waves are monochromatic, unidirectional waves which satisfy several fundamental boundary conditions. The first is the combined linear free surface boundary condition which places kinematic restrictions on the fluid particles along the free surface and dynamic restrictions on the pressure along the free surface. Plane progressive waves also satisfy the sea floor condition which states that fluid particles cannot penetrate the bottom boundary of the fluid domain. Finally, plane progressive waves satisfy Laplace's equation

$$\nabla^2 \phi = 0 \tag{4}$$

where ϕ is the scalar potential defining plane progressive waves. By the linearity of the Laplacian operator ∇^2, if $\nabla^2 \phi_1 = 0$ and $\nabla^2 \phi_2 = 0$, then

$$\nabla^2(\phi_1 + \phi_2) = \nabla^2 \phi_1 + \nabla^2 \phi_2 = 0$$

Thus, potential flow solutions can be superimposed to yield more complicated solutions.

Define A the wave amplitude, ω the wave frequency, k the wavenumber, and ε the wave phase. Then the velocity field for plane progressive waves $\boldsymbol{V}_{\mathrm{f}}$ (expressed in the Earth-fixed frame) is given by

$$\boldsymbol{V}_{\mathrm{f}}(x, z, t) = A\omega e^{-kz} \begin{pmatrix} \cos(kx - \omega t + \varepsilon) \\ 0 \\ -\sin(kx - \omega t + \varepsilon) \end{pmatrix} \tag{5}$$

To express the velocity field in the body frame, the transformation $\boldsymbol{v}_{\mathrm{f}} = \boldsymbol{R}^T \boldsymbol{V}_{\mathrm{f}}$ can be used. In this formulation (5), the wavelength is aligned with the i_1 axis and the wave exhibits exponential decay in the i_3 direction. A snapshot over one wavelength is given in Figure 1. A more inclusive discussion of plane progressive waves can be found in chapter 6 of [14].

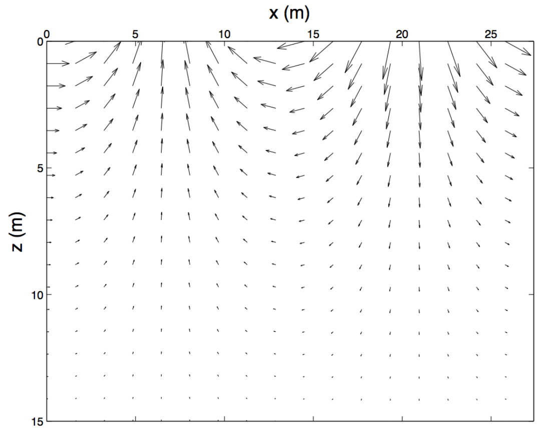

Fig. 1. A snapshot of the velocity field for plane progressive waves.

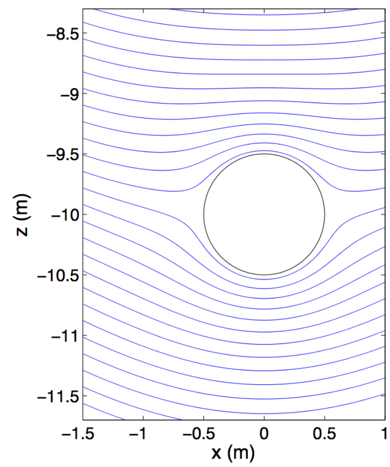

Fig. 2. Streamlines plotted over the potential flow cylinder in plane progressive waves.

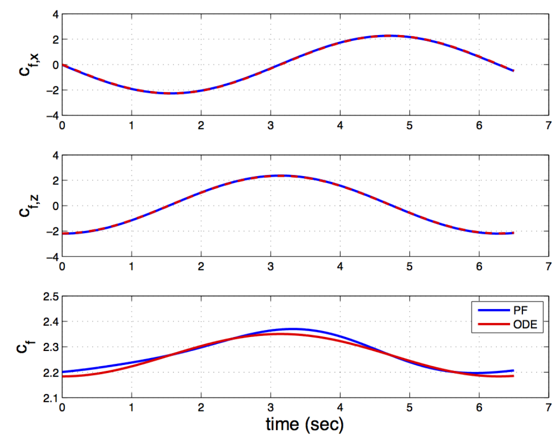

Fig. 3. A comparison between the force coefficients and magnitude computed by the analytic potential flow solution and those predicted by the model dynamics. Force coefficients are compared in the i_1 direction (top), the i_3 direction (middle), and the magnitude is compared (bottom).

B. *Model comparison in Plane Progressive Waves*

Before continuing to the formulation of the natural seaway, the model (3) is compared to an exact potential flow solution. This comparison examines the case of a 2-dimensional cylinder held stationary in plane progressive waves. The Milne-Thomson circle theorem [15] is used to establish additional boundary conditions consistent with the presence of a cylinder fixed within the fluid domain. This is illustrated in Figure 2 where streamlines have been plotted over the body. The pressure can be computed over the cylinder surface using the unsteady Bernoulli equation and then integrated over the body to yield the corresponding force coefficients in the vertical and horizontal directions. These forces are then compared to those predicted by the dynamic model defined for the same scenario. The resulting comparison, in Figure 3, reveals almost identical results in the vertical and horizontal directions. When the force coefficient magnitude is computed, the disparity is noticeable because of the tighter bound on the y-axis limits.

It should be noted that this comparison only captures Froude-Krilov forces. While the analytical cylinder satisfies a kinematic boundary condition such that the fluid particles do not pierce the surface of the cylinder, it does not satisfy a radiation condition. Thus, it does not inherently account for energy dissipation in the form of radiated waves.

C. *Modeling a Natural Seaway*

As modeled in this effort, the natural seaway uses the Pierson-Moskowitz wave energy density spectrum which models a fully developed sea in the North Atlantic [8]. The Pierson-Moskowitz one-parameter spectrum

$$S(\omega) = \frac{8.1 \times 10^{-3} g^2}{\omega^5} \exp\left[-0.74 \left(\frac{g}{U\omega}\right)^4\right] \tag{6}$$

is a function of the wind speed U (as measured from 19.5 m above sea level). The spectrum is plotted for wind speeds of 5ms^{-1}, 10ms^{-1}, 15ms^{-1}, 20ms^{-1} in Figure 4.

The area under a the spectral density curve is the mean-square of the wave height. Using this, the wave spectrum can be approximated with a superposition of plane progressive waves as follows. First, select a wind velocity and a set of interpolation frequencies where the spectral density curve is nonzero. These will ultimately be the frequencies of the superimposed waves. Next, approximate the area under the spectral density curve using a Riemann sum. For an approximation using rectangular slices, the area of each slice is $S(\omega_i)\Delta\omega_i$. The term $S(\omega_i)$ represents the height at the i^{th} interpolation frequency and the term $\Delta\omega_i$ represents the corresponding width, *i.e.* the distance between successive interpolation frequencies. Then each of the wave amplitudes can be computed as

$$A_i = \sqrt{2S(\omega_i)\Delta\omega_i} \tag{7}$$

Lastly, generate a random phase ε_i for each wave. The resulting free surface corresponding to a Pierson-Moskowitz spectrum with a wind speed of 10ms^{-1} ($\sim$20 knots) and 15 frequencies evenly spaced on $\omega = [0.6, 2]$ is plotted in Figure 5.

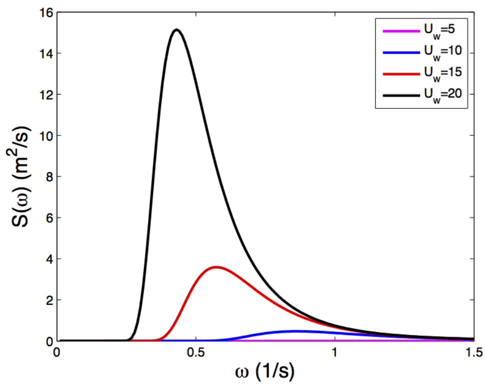

Fig. 4. The Pierson-Moskowitz spectrum (6) plotted for wind speeds of 5ms^{-1}, 10ms^{-1}, 15ms^{-1}, 20ms^{-1}.

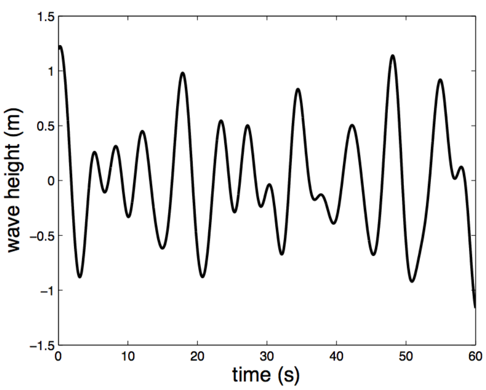

Fig. 5. The free surface for a Pierson-Moskowitz spectrum with a wind speed of 10ms^{-1} and 15 evenly space frequencies between 0.6s^{-1} and 2s^{-1}.

IV. Simulations

A. Vehicle Parameters

Take the vehicle to be an ellipsoid with three distinct semi-axes. The vehicle is assumed to be neutrally buoyant with its center of mass below the center of buoyancy along the b_3 axis such that the vehicle is bottom-heavy. The vehicle is underactuated with a propulsion system and four stern planes arranged in a cruciform configuration giving control authority in the surge, pitch, and yaw directions. (The stern planes opposite to eachother are assumed to move in unison so as to only allow control moments in the pitch and yaw directions.) Further, we impose saturation limits on the stern planes to approximate hydrodynamic stall and actuator limitations. Actuator dynamics are not modeled and control authority is assumed to be applied instantaneously. Additionally, complex hydrodynamic effects like flow separation and actuator added mass are not considered.

Lift and drag are modeled following the work in [6]. (In particular, see Remark 2.3 in [6].) Drag parameter values are approximated from [16] and the drag model assumes that the vehicle is subject to quasi-steady flow. While this assumption is not ideal, it is expected that the resulting impact on the dynamics does not transcend the effects of the previous modeling assumptions. We expect that experimental data, taken from a similar maneuvering envelope to that of this effort, could yield more accurate approximations of these values.

The explicit parameter values employed in this paper are summarized in Table I. For the case of a natural seaway, the background flow field is defined according to Figure 5. When simulating plane progressive waves, all of the wave energy is assumed to be condensed to a single frequency.

TABLE I

Constants used to initialize control simulations.

Parameter	Value	Parameter	Value
Vehicle length, L	2m	Vehicle beam, B	0.27m
Vehicle mass, m	88.7kg	Vehicle draft, D	0.30m
Parasite drag, C_{d0}	0.28	Induced drag, C_{d1}	0.0056
Roll damping, τ_ϕ	0.1N·m·s	Lift curve slope, $C_{l\alpha}$	0.15
Pitch damping, τ_θ	0.1N·m·s	Yaw damping, τ_ψ	0.1N·m·s
CM location, $r_{\rm cm}$	0.04m	SP location, $r_{\rm sp}$	0.8m

B. Control Objective

To demonstrate the capabilities of the proposed model, we examine the problem of depth tracking, illustrated in Figure 6. To achieve this objective, the desired depth $z_{\rm d}$ and the look ahead distance $k_x L$ are used to establish a desired pitch orientation $\theta_{\rm d}$ such that the vehicle will converge to the desired depth. To explore the full six degrees of freedom of the model, a prescribed heading angle $\psi_{\rm d}$ relative to the direction of wave propagation is implemented. In the illustration (Figure 6), this would correspond to the vehicle coming out of the page by an angle $\psi_{\rm d}$.

To carry out the control objective, a simple proportional derivative (PD) controller is implemented in the pitch and yaw directions:

$$\boldsymbol{\tau}_{\rm c} = \begin{pmatrix} 0 \\ \tau_\theta \\ \tau_\psi \end{pmatrix} = \begin{pmatrix} 0 \\ k_{\rm p}^{\theta}(\theta_{\rm d} - \theta) - k_{\rm d}^{\theta}\dot{\theta} \\ k_{\rm p}^{\psi}(\psi_{\rm d} - \psi) - k_{\rm d}^{\psi}\dot{\psi} \end{pmatrix} \tag{8}$$

A constant thrust f_u is applied along the surge direction and the resulting control force is

$$\boldsymbol{f}_{\rm c} = \begin{pmatrix} f_u \\ -\tau_\psi / r_{\rm sp} \\ -\tau_\theta / r_{\rm sp} \end{pmatrix} \tag{9}$$

where the forces in sway and heave are incurred from control moments normalized by the moment arm $r_{\rm sp}$, which represents the distance from the stern plane's point of action to the center of gravity.

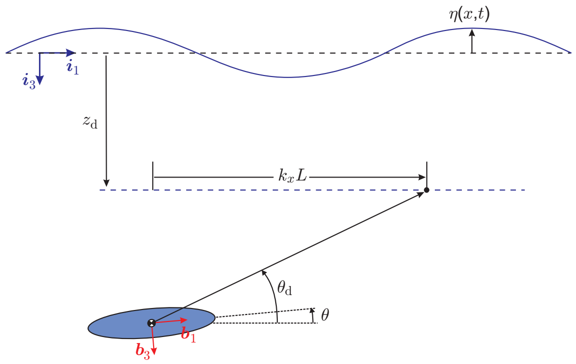

Fig. 6. Illustration of the control objective projected into the plane of the waves.

TABLE II
CONTROL PARAMETER VALUES.

Parameter	Value	Parameter	Value
Proportional gain, k_{p}^{θ}	$800_{\mathrm{N\cdot m}}$	Derivative gain, k_{d}^{θ}	$500_{\mathrm{N\cdot m\cdot s}}$
Proportional gain, k_{p}^{ψ}	$800_{\mathrm{N\cdot m}}$	Derivative gain, k_{d}^{θ}	$500_{\mathrm{N\cdot m\cdot s}}$
Thrust, f_u	50_{N}	Saturation limit	$69.6_{\mathrm{N\cdot m}}$
Look ahead, k_x	3		

C. Results

1) Simulation in Plane Progressive Waves: The simulation was initialized with all initial states equal to zero, except for the initial depth of 12m, and desired depth and heading of 10m and 10 degrees, respectively. The resulting state histories for simulation in plane progressive waves are given in Figure 7. The vehicle behavior is initially characterized by a transient period where the pitch angle is regulated towards the desired value and the vehicle approaches the desired depth. After 15s, the vehicle settles into a steady state oscillation about the desired depth. This is a result of the vehicle's inability to predict and reject disturbances from the unsteady flow field. It is suggested by the authors that feedforward disturbance rejection could be used to effectively mitigate the steady state oscillations.

The dynamics in the yaw direction are rather benign, as one might expect. As discussed in Section III-A, all of the background flow dynamics take place in the (i_1, i_3) plane. However, the resulting small scale oscillations are a result of the dynamic coupling between the six degrees of freedom. However, these effects are small in comparison to the wave forcing, so the yaw tracking controller is able to maintain the desired heading with relative ease.

2) Simulation in a Natural Seaway: The natural seaway was approximated using 15 superimposed plane progressive waves, according to Figure 5 and the simulation was initialized with the same conditions as before. Similar to the simulation in plane progressive waves, the vehicle initially experiences a transient period where the vehicle acclimates to the desired depth. However, in this case, the vehicle does not fall into the oscillatory, steady state motion as in Figure 7. Since the pitch controller in Figure 8 tracks the desired pitch as well as the controller in plane progressive waves, the resulting inconsistency in the depth performance can be attributed to the prescribed flow field. Essentially, this is a result of the randomness of the fluid motion in a natural seaway.

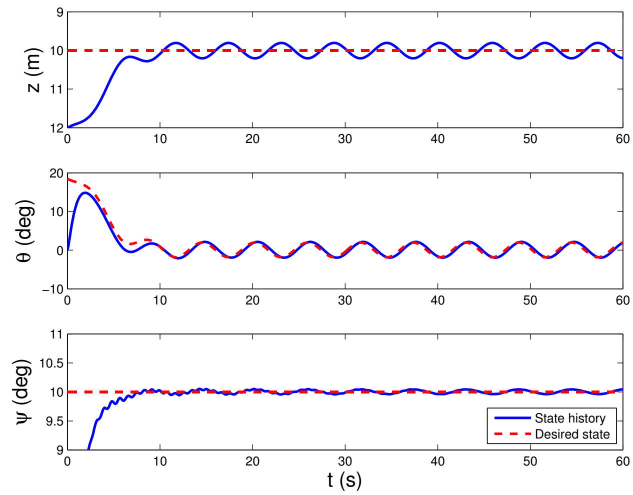

Fig. 7. Results for an underwater vehicle operating in plane progressive waves. Depth tracking is shown in the top plot, pitch tracking in the middle plot, and heading tracking in the bottom plot. Note the heading angle ψ begins at zero, but the y-axis limits are narrowed to make the unsteady coupling effects more visable

The yaw dynamics perform in a similar fashion to the case in plane progressive waves. There are noticeable perturbation spikes in the yaw history, however. These seem to correspond with amplified motion in the other degrees of freedom, again as a result of the coupled dynamics.

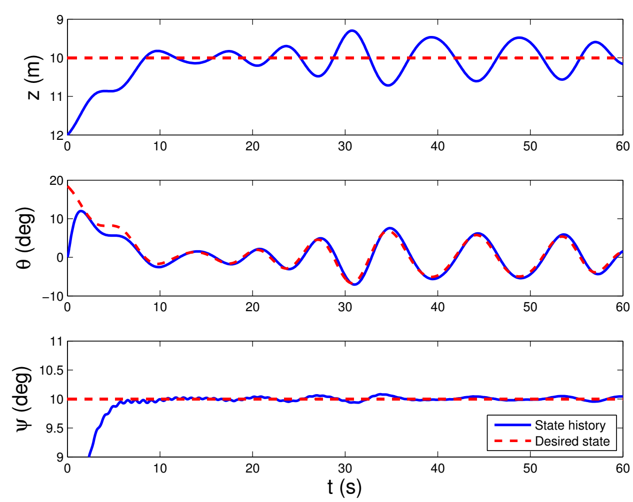

Fig. 8. Results for an underwater vehicle operating in a natural seaway. Depth tracking is shown in the top plot, pitch tracking in the middle plot, and heading tracking in the bottom plot.

V. Conclusions

To recap, the underwater vehicle model derived in [11] was specialized to the case of a vehicle operating in plane progressive waves. After comparing the predicted forces for the case of a two-dimensional cylinder, and demonstrating that the model could accurately capture Froude-Krylov forces, the model was extended to represent the effect of a natural seaway. The natural seaway was constructed by approximating the Pierson-Moskowitz wave spectrum using a finite number of plane progressive waves.

Simulation results were compared between two cases: an underwater vehicle operating in plane progressive waves and a vehicle operating in a natural seaway. While the former case exhibits a transient period followed by steady state oscillation, the random seas in the latter case prevent such steady state motions.

While the proposed model has not been validated against high-fidelity CFD or experimental results, the favorable comparison with analytical results for simple geometries is promising. In addition to validating the model, ongoing work includes modeling seakeeping effects such as frequency dependent added mass and radiative damping. While it is relatively straightforward to implement frequency dependent added mass and damping for the case of a single wave, it is not trivial to extend this approach to a natural seaway. This especially true for nonlinear dynamic models where superposition cannot be invoked.

Acknowledgements. The authors gratefully acknowledge the advice and guidance of Dr. Eric Paterson, Dr. Leigh McCue-Weil, Dr. Francis Valentinis, Dr. Tristan Perez, and Dr. Ron Joslin and the sponsorship of the Office of Naval Research under Grant No. N00014-14-1-0651.

References

[1] P. A. Bailey, W. G. Price, and P. Temarel, “A unified mathematical model describing the manoeuvring of a ship travelling in a seaway,” in *Trans. RINA*, vol. 140, 1998, pp. 131–149.

[2] T. I. Fossen, “A nonlinear unified state-space model for ship maneuvering and control in a seaway,” *Journal of Bifurcation and Chaos*, vol. 15, no. 9, pp. 2717–2746, September 2005.

[3] T. Perez, *Ship Motion Control: Course keeping and roll stabilisation using rudder and fins*. Springer, 2005.

[4] N. E. Leonard, “Stability of a bottom-heavy underwater vehicle,” *Automatica*, vol. 33, no. 3, pp. 331–346, 1997.

[5] ——, “Stabilization of underwater vehicle dynamics with symmetry-breaking potentials,” *Automatica*, vol. 32, pp. 35–42, 1997.

[6] C. A. Woolsey and L. Techy, “Cross-track control of a slender, underactuated AUV using potential shaping,” *Ocean Engineering*, vol. 36, pp. 82–91, 2009.

[7] F. Valentinis, A. Donaire, and T. Perez, “Energy-based motion control of a slender hull unmanned underwater vehicle,” *Ocean Engineering*, vol. 104, pp. 604–616, June 2015.

[8] T. I. Fossen, *Guidance and Control of Ocean Vehicles*. New York: Wiley, 1994.

[9] B. J. Racine and E. G. Paterson, “CFD-based method for simulation of marine-vehicle maneuvering,” in *35th AIAA Fluid Dynamics Conference and Exhibit*. Toronto, Ontario Canada: AIAA, June 20015.

[10] P. G. Thomasson, “Equations of motion of a vehicle in a moving fluid,” *Journal of Aircraft*, vol. 37, no. 4, pp. 630–639, August 2000.

[11] P. G. Thomasson and C. A. Woolsey, “Vehicle motion in currents,” *IEEE Journal of Oceanic Engineering*, vol. 38, no. 2, pp. 226–242, April 2013.

[12] H. Lamb, *Hydrodynamics*. Dover Publications, 1932.

[13] J. H. Milgram, “Strip theory for underwater vehicles in water of finite depth,” *Journal of Engineering Math*, vol. 58, pp. 31–50, 2007.

[14] J. N. Newman, *Marine Hydrodynamics*. Cambridge, MA: The MIT Press, 1977.

[15] L. M. Milne-Thomson, *Theoretical Hydrodynamics Fourth Edition*. St. Martin’s Press Inc., 1960.

[16] S. F. Hoerner, *Fluid Dynamic Drag*, Hoerner, Ed. Midland Park, NJ: Hoerner, 1965.